Acknowledgment. We gratefully acknowledge the financial assistance of the National Research Council of Canada's Operating, New Ideas and Strategic Energy programs, Imperial Oil of Canada, Erindale College, and Lash Miller Chemical Laboratories for support of this research.

Registry No. Hf, 7440-58-6; W, 7440-33-7; Re, 7440-15-5; Ru, 7440-18-8; Zr, 7440-67-7; Pd, 7440-05-3; Au, 7440-57-5; Zr_2, 12597-66-9; Pd_2, 12596-93-9; Au_2, 12187-09-6; Au_3, 75024-07-6.

Contribution from Lash Miller Chemical Laboratories and Erindale College, University of Toronto, Toronto, Ontario, Canada M5S 1A1

Very Small Bimetallic Clusters of Silver with Manganese, Molybdenum, and Copper in Rare Gas Matrices

W. E. KLOTZBÜCHER and G. A. OZIN*

Received December 28, 1979

The simultaneous codeposition of silver vapor with manganese, molybdenum, and copper vapor in low-temperature argon matrices at 10–12 K provides a synthetic pathway to low-nuclearity, bimetallic clusters, some of which are of the low-miscibility class in the respective binary alloy systems. Mixed-metal concentration, annealing, and selective photoaggregation studies in combination with optical absorption spectroscopy allow the tentative identification of AgMn, AgMo, and AgCu molecules as well as some less well-defined, higher bimetallic clusters. A preliminary view of the electronic and bonding architecture of these bimetallic combinations is obtained from extended Hückel calculations, and some comments are forwarded on the relevance of these studies to concepts in the field of alloy and bimetallic cluster catalysis.

Introduction

The interactive electronic architecture which has recently emerged from the very low-nuclearity cluster systems Cr_nMo_m[1] and Cr_nAg_m[2] entrapped within weakly interacting, low-temperature supports has provided an interesting new perspective with which to view highly dispersed, multimetallic cluster catalysts comprised of partially immiscible or wholly immiscible components.[3] In contradistinction, the striking, noninteractive characteristics observed at the atomic level for the Pd/Ag and Pd/Mo[4] combinations alert one to the fact that the simple mixing of metal atomic vapors under cryogenic conditions is not sufficient to ensure reactive encounters and the formation of bimetallic clusters. Clearly, more subtle factors of an electronic and kinetic nature can contribute to and markedly affect the early stages of bimetallic cluster growth at low temperatures, even though the respective bulk-phase diagrams may imply total miscibility of the metallic components over the entire concentration range.[5]

For determination of the generality of the above observations and the scope of the method for synthesizing controlled-size, multimetallic clusters for spectroscopic, theoretical, and chemical investigations, a systematic study of a wide range of metallic combinations needs to be undertaken. The basic requirements for progress in this area are, first, fairly well-understood parent cluster systems and, second, minimal spectral interference of atomic and cluster species in the two-component systems. In this context, the small cluster systems $Cu_{2,3}$,[6] $Ag_{2,3}$[6b,7] and $Mo_{2,3}$[1,8] are reasonably well suited for bimetallic undertakings.

Following up on some earlier matrix work which suggested anomalously facile aggregation pathways in the Mn/CO system[9] (e.g., Mn/CO $\simeq$ 1/10[3] yields almost exclusively $Mn_2(CO)_{10}$ at 10–12 K), it was thought worthwhile to elucidate the aggregation characteristics of Mn in rare gas matrices (thereby completing the cluster studies of the first transition series[10]) with an extension to bimetallic combinations. The results obtained with the metallic pairs Ag/Mn, Ag/Mo, and Ag/Cu will be described in this paper, the unifying theme being the presence of silver in all three systems investigated.

Experimental Section

Our experimental setup for metal and bimetal vapor depositions has been described previously.[1] Monoatomic metal vapors were generated by direct resistive heating (ac) of either a metal filament (Mo), a tungsten support (Cu), or a tantalum Knudsen cell (Ag, Mn) suspended between two water-cooled electrodes. Tungsten supports and tantalum Knudsen cells were manufactured in the University of Toronto workshops without the use of oil-based solvents and were thoroughly outgassed in vacuo before use. (Manganese evaporation from graphite Knudsen cells treated identically showed similar results.) The metals were of better than 99.99% purity, with the metal flow quantitatively and continuously monitored by a dual quartz-crystal microbalance assembly. The matrix gas flow was controlled by a calibrated micrometer needle valve and thermocouple vacuum gauge assembly. A Displex closed-cycle helium refrigerator was used to cool a NaCl optical window to 10–12 K, the temperature being monitored by a Au–0.07 atom % Fe thermocouple embedded in a drilled cavity

(1) W. E. Klotzbücher and G. A. Ozin, *J. Am. Chem. Soc.* **100**, 2262 (1978); *J. Mol. Catal.*, **3**, 195 (1977); W. E. Klotzbücher, G. A. Ozin, J. G. Norman, Jr., and H. J. Kolari, *Inorg. Chem.*, **16**, 3871 (1977).
(2) W. E. Klotzbücher and G. A. Ozin, *Inorg. Chem.*, **18**, 2101 (1979).
(3) J. H. Sinfelt and J. A. Cusumano in "Advanced Materials in Catalysis", J. J. Burton and R. L. Garten, Eds., Academic Press, New York, 1977; J. H. Sinfelt, *Acc. Chem. Res.*, **10**, 15 (1977), and references cited therein.
(4) W. E. Klotzbücher and G. A. Ozin "Photoselective Bimetallic Aggregation", Proceedings of the NBS Conference on High Temperature Science, Washington, D.C., 1978.
(5) M. Hansen, "Constitution of Binary Alloys", McGraw-Hill, New York, 1958, and supplements.
(6) (a) M. Moskovits and J. Hulse, *J. Chem. Phys*, **67**, 4271 (1977); (b) G. A. Ozin, H. Huber, D. McIntosh, S. Mitchell, J. G. Norman, Jr., and L. Noodelman, *J. Am. Chem. Soc.* **101**, 3504 (1979).
(7) H. Huber and G. A. Ozin, *Inorg. Chem.*, **17**, 155 (1978); G. A. Ozin and S. Mitchell, *J. Am. Chem. Soc.*, **100**, 6776 (1978); *Inorg. Chem.*, **18**, 2932 (1979); W. Schulze, H. U. Becker, and H. Abe, *Chem. Phys.*, **35**, 177 (1978); T. Welker and P. T. Martin, *J. Chem. Phys.*, **70**, 5683 (1979); D. M. Gruen and J. K. Bates, *Inorg. Chem.*, **16**, 2450 (1977).
(8) W. E. Klotzbücher and G. A. Ozin, *Inorg. Chem.*, **16**, 984 (1977).
(9) G. A. Ozin, H. Huber, E. P. Kündig, and A. J. Poë, *J. Am. Chem. Soc.*, **97**, 308 (1975).
(10) W. E. Klotzbücher, Ph.D. Thesis, "Bimetal Vapour Chemistry", University of Toronto, 1979.

0020-1669/80/1319-3776$01.00/0

close to the window center. UV–visible spectra were recorded on a standard Unicam SP 8000 spectrometer in the range 200–700 nm. For the photochemical experiments, the output of a 450-W Oriel xenon lamp was focused through a constant-temperature, 10-cm water cell onto the entrance slit of a Schoeffel GM 100 grating monochromator.

To metal atom chemists, manganese has a history of being "strange" under cryochemical conditions and has always had the reputation of being the odd-man-out in the first transition series. The paucity of manganese atom papers, attests to the problems which have been previously experienced at both the matrix and macropreparative scales of operation with this element. This situation relates to a number of peculiar properties of manganese atoms such as surprisingly facile matrix aggregation behavior,[9] low-yield reaction chemistry, low sticking coefficient,[10] high promotion energies from the $3d^5 4s^2\ ^6S_{5/2}$ electronic ground state,[11] and a van der Waals dimer,[12] to name a few. Manganese is tricky, and in some ways temperamental, but we believe that our paper goes part way toward clarifying why and where difficulties exist in handling the vapors of the element under cryogenic conditions.

We would like to emphasise that the spectral data for all systems reported in our paper are highly reproducible from run to run. This aspect of the investigation was particularly carefully scrutinized because of our awareness of the problems associated with manganese in both uni- and bimetallic applications.[13] Great care was taken to examine each system under a wide range of reaction conditions, checking reproducibility as well as looking for any extraneous effects associated with the usual contaminants which tend to emanate from vaporization sources, furnaces, and vacuum systems. In addition we have employed every technique that we know to establish the isolation and aggregation characteristics of manganese atoms in rare gas supports. Taking the study in its entirety, we believe that our assignments and deductions are reasonable and represent a useful first attempt at understanding one of the most problematical metal atomic–cluster systems in the transition group.

Results

Manganese. Manganese was one of the first metals to be investigated by the matrix isolation method. Schnepp and others,[14,15] utilizing photographic detection methods, identified two major absorptions in the 275- and 400-nm regions, shifted only slightly from the gas-phase positions.[11] Two later studies using photoelectric detection techniques were hampered by base line irregularities, especially in the UV region of the spectrum, as well as by the accidental trapping of higher clusters.[16] For the more intense bands the agreement between these authors is quite good. However, the behavior of weaker absorptions in the system appears somewhat erratic.

Preliminary control experiments in the present study, involving manganese evaporation from carefully outgassed tantalum and graphite Knudsen cells, although always displaying some visual signs of manganese oxide formation in the cell (presumably from residual oxygen occluded in or chemisorbed on the manganese powder), confirmed that the absorptions which could not be accounted for as matrix-entrapped manganese atoms were not those of extraneous MnO_x molecules.[17] An interesting phenomenon was noticed during these initial depositions concerning the anomalous sticking properties of manganese atoms impinging on the quartz-crystal mass monitor. Apparently the accommodation coefficient of manganese on the surface of the microbalance is dependent on the thickness of the deposited film as well as on the rate of metal deposition (similar "atom-bouncing" problems have been experienced with macroscale reactions of manganese vapor with liquid reagents in rotary reactors[18] and probably have their origin with the symmetrical $3d^5 4s^2$ ground state of Mn). Consequently our attempts to unequivocally identify manganese dimer and higher cluster optical absorptions from quantitative metal concentration experiments[19] were foiled, and the data have to be treated in a more qualitative manner. Nevertheless by careful selection of reaction conditions a considerable amount of useful information can be extracted

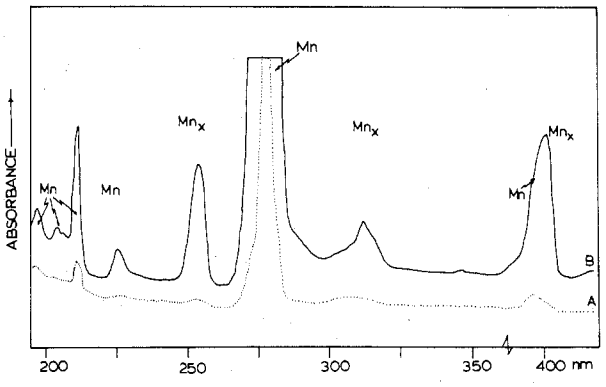

Figure 1. UV–visible spectrum of a Mn/Ar ≃ $1/10^4$ mixture deposited at 10–12 K showing (A) the major Mn atom lines and (B) the enhancement of weak lines by prolonged deposition. The assignment of Mn_x and Mn_y is discussed in the text.

Table I. Band Assignments, Matrix Shifts, and Electronic Configurations for Matrix-Isolated Manganese Atoms (Ground State $3d^5 4s^2$; $^6S_{5/2}$)

Ar matrix[a]			shift[a]							
λ, nm	ν, cm^{-1}	gas ν, cm^{-1}	Δν, cm^{-1}	3d	4s	4p	5p	S	L	J
		0		5	2	0	0	6	0	$^5/_2$
197	50 800	50 099	−744	5	1	1	0	6	1	$^3/_2$
		50 013		5	1	1	0	6	1	$^5/_2$
203	49 300	49 888	588	5	1	1	0	6	1	$^7/_2$
211	47 400	47 782	382	5	1	0	1	6	1	$^3/_2$
		45 259		6	0	1	0	6	1	$^3/_2$
226	44 300	45 156	836	6	0	1	0	6	1	$^5/_2$
		44 994		6	0	1	0	6	1	$^7/_2$
		35 770		5	1	1	0	6	1	$^7/_2$
277	36 100	35 726	−371	5	1	1	0	6	1	$^5/_2$
		35 690		5	1	1	0	6	1	$^3/_2$
		24 802		5	1	1	0	6	1	$^7/_2$
392	25 500	24 788	−710	5	1	1	0	6	1	$^5/_2$
		24 779		5	1	1	0	6	1	$^3/_2$

[a] Accuracy of the matrix wavenumber positions estimated to be ±100 cm^{-1}.

Table II. Position and Assignment of Manganese Cluster Absorptions

Ar[a]		Kr[a]		
λ, nm	ν, cm^{-1}	λ, nm	ν, cm^{-1}	assignt
253	39 500	254	39 400	Mn_x
312	32 000	317	31 500	Mn_x
400	25 000	410	24 400	Mn_x
650	15 400	670	14 900	Mn_2
329	30 400	332	30 100	Mn_y
		336	29 800	
345	29 000	349	28 700	Mn_y
288	34 700	290	34 500	Mn′
435	23 000	444	22 500	Mn′

[a] Accuracy of the matrix wavenumber positions estimated to be ±100 cm^{-1}.

(11) D. H. W. Carstens, W. Brashear, D. R. Eslinger, and D. M. Gruen, *Appl. Spectrosc.*, **26**, 184 (1972).
(12) A. Kant, S. Lin, and B. Strauss, *J. Chem. Phys.*, **49**, 2765 (1965).
(13) W. Dyson and P. A. Montano, *J. Am. Chem. Soc.*, **100**, 7439 (1978).
(14) O. Schnepp, *J. Phys. Chem. Solids*, **17**, 188 (1961).
(15) E. L. Lee and R. G. Gutmacher, *J. Phys. Chem. Solids*, **23**, 1823 (1962).
(16) (a) D. M. Mann and H. P. Broida, *J. Chem. Phys.*, **55**, 84 (1971); (b) W. R. Graham and W. W. Duley, *ibid.*, **55**, 2527 (1971).
(17) K. R. Thompson, W. C. Ensling, and L. B. Knight, *J. Phys. Chem.*, **77**, 49 (1973).
(18) C. F. Francis and P. L. Timms, private communication.
(19) M. Moskovits and J. Hulse, *J. Chem. Soc., Faraday Trans. 2*, 471 (1977).

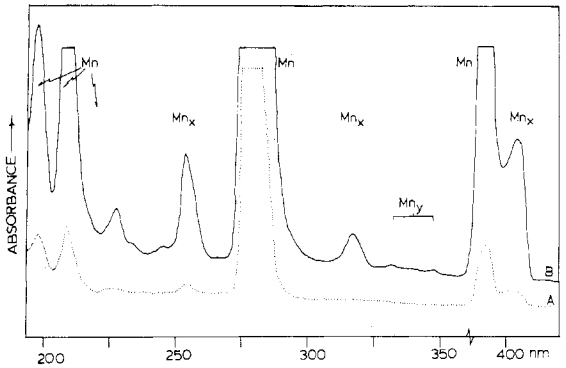

Figure 2. (A) UV–visible spectrum of a Mn/Kr ≃ $1/10^4$ mixture obtained with very slow metal deposition rates. (B) Spectrum of the mixture after prolonged deposition showing the presence of Mn_x and Mn_y.

Table III. Absorptions Associated with Unimetallic and Bimetallic Clusters of Silver, Copper, Manganese, and Molybdenum in Rare Gas Matrices

molecule	abs, nm	molecule	abs, nm
		Krypton	
Ag_2	275/278, 389	Mn_2	670
Ag_3	222/232/246, 422	Mn_x	254, 317, 410
Ag_4	286, 524	Mn_y	332, 336, 349
Ag_5	349, 476	AgMn	(236/240/244), 263/266, 362
Ag_6	366, 508	Ag_xMn_y	492, 502, 550, 592, 604
		Argon	
AgMo	432/440	AgCu	271, 382
Mo_2	232, 308, 518	Cu_2	219/222, 230/235/239, 262, 360

from the matrix spectra at the very early stages of manganese cluster growth.

Let us initially focus attention on the optical spectrum obtained on depositing Mn/Ar mixtures at an estimated dilution of $1/10^4$ at 10–12 K displayed in Figure 1A. Aside from the two known band systems at 277 and 392 nm,[11,14,15] a hitherto unobserved atomic system could be detected in the 190–226-nm region under prolonged deposition conditions (Figure 1B). These high-sensitivity scans also revealed a group of weaker absorptions around 253, 312, and 400 nm which do not appear to be associated with atomic manganese. The 400-nm band is better resolved in Kr matrices. See Figure 2. The results for Mn/Kr high-dilution samples deposited at 10–12 K are quite similar (Figure 2), although the relative intensities of the aforementioned weak absorptions could be reduced compared to Mn/Ar. Spectra entirely free of these "nonatomic" bands could not be obtained. Table I lists the energies and electronic assignments of the absorptions assignable to manganese atoms.

As mentioned earlier, weak absorptions at 253, 312, and 400 nm in Ar cannot be associated with atomic species and are unlikely to represent unstable atomic sites. The suspicion that these absorptions could be ascribed to Mn_2 contradicts an earlier literature report which placed the spectrum of Mn_2 at 650 nm in Ar.[20] Controlled annealing and metal concentration experiments in Ar and Kr were quite informative in this regard (Figures 2–4). For example, 20 K warming in Kr effected marked spectral alterations where the absorptions at 254, 317, and 410 nm grew in rapidly with concomitant loss of Mn atom

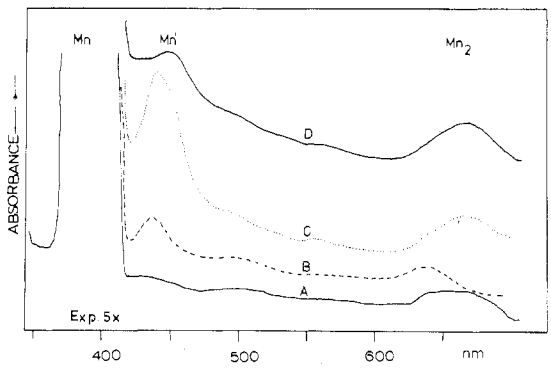

Figure 3. Low-energy region of a Mn/Kr ≃ $1/10^4$ mixture (A) after deposition at 10–12 K, (B) on annealing at 20 K, (C) upon scanning at 10–12 K after annealing to 28 K, and (D) after Mn atom irradiation (absorbance scale, 5× expanded).

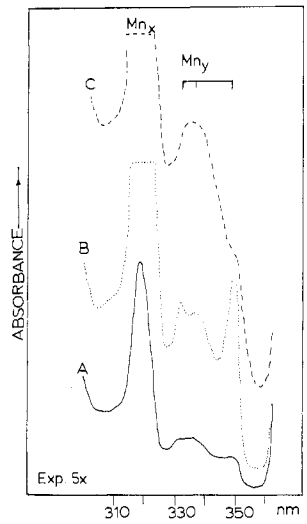

Figure 4. UV–visible spectra of the weak absorptions assigned Mn_y (A) on deposition in krypton, (B) upon scanning after annealing to 25 K, and (C) after cooling back to 10–12 K, showing the temperature dependence of the 349-nm absorption (absorbance scale, 5× expanded).

intensity. Furthermore, a number of new, weak features emerged above 400 nm and between 325 and 350 nm (Figures 3 and 4). The remarkably clear feature at 444 nm grew in rapidly on warm-up (Figure 3B,C) and paralleled the behavior of a 290-nm shoulder on the major Mn absorption. Narrow-band, 275-nm atomic excitation resulted in the loss of both the 444- and 290-nm lines (Figure 3D) which could be restored upon thermal annealing at 20 K. Such behavior has been observed recently in the silver atom–rare gas system[21] and is best attributed to a matrix site redistribution effect involving major and minor manganese atom sites, Mn and Mn′, respectively. Interestingly, the purported 650-nm Mn_2 band[20] can be generated in higher metal concentration experiments at 650 nm in Ar and 670 nm in Kr (Figure 3A). The band maximum shifts toward the blue at 15–20 K (Figure 3B) and increases in intensity upon warming to 30 K (Figure 3C). However, $3d^54s^2 \rightarrow 3d^54s4p$ Mn atom photoexcitation caused little change in the spectrum (Figure 3D). Although concentration studies were attempted, for reasons described earlier, they did not allow a clear definition of cluster nuclearity. For consistency the 650–670-nm feature is labeled Mn_2 (Figure 3). The behavior of the species labeled Mn_x and Mn_y appears to be characteristic of small clusters which can be generated

(20) T. C. DeVore, A. Ewing, H. F. Franzen, and V. Calder, *Chem. Phys. Lett.*, **35**, 78 (1975).

(21) G. A. Ozin, S. Mitchell, J. Farrell, and G. Kenney-Wallace, *J. Am. Chem. Soc.*, in press.

by surface and bulk annealing but apparently not by photoaggregation methods. Although the intensity behavior of the Mn_x species (which can safely be assigned a lower nuclearity than Mn_y) is different from the purported Mn_2 absorption at 650–670 nm,[20] it is conceivable that under the high-dilution conditions chosen both sets of absorptions represent dimanganese. On this point it is significant that ab initio HF molecular orbital calculations[22] predicted an essentially equienergetic set of different spin states for ground-state Mn_2 which might possibly be *coisolated* in cryogenic trapping experiments of the type described. Further studies will be required to clarify this intriguing proposition.

The group of absorptions designated Mn_y which appear weakly in the higher concentration experiments exhibit some unusual temperature-dependent effects. For example, the three major Mn_y features in Kr at 332, 336, and 349 nm (Figure 4) grow upon thermal annealing to 25 K but with the 349 nm absorption displaying completely reversible, temperature-dependent intensity effects (Figures 4B,C) upon temperature cycling in the range 10–25 K. Although the growth patterns of the Mn_y species from annealing and concentration studies point toward a nuclearity of greater than 2, further studies will be required to establish the exact value of y as well as the origin of the interesting temperature dependence of the spectrum.

It is clear from the above experiments that Mn atom aggregation under matrix cryogenic conditions is an extremely facile process and one that is essentially impossible to avoid even under circumstances which usually favor exclusive isolation of metal atomic species.[10] With hindsight it is therefore not too surprising that the matrix infrared spectrum of the products formed on cocondensing manganese vapor with pure CO revealed $Mn_2(CO)_{10}$ with only minor quantities of $Mn(CO)_5$.[9]

Silver–Manganese Bimetal Vapor Studies. The aggregation properties of silver and manganese induced by surface, bulk, and photodiffusion procedures show some differences. In brief, silver atoms can be easily matrix isolated but can also be induced to cluster readily, and in a controlled manner, by deposition, annealing, and photoaggregation procedures.[7] On the other hand, surface diffusion–aggregation pathways for Mn during deposition are extremely facile and, as mentioned, prevent effective atomic isolation at 10–12 K. Moreover, bulk diffusion and rapid agglomeration of Mn are favored processes even in rigid matrices, while Mn atom photoexcitation appears to be an ineffective means of generating manganese clusters.

With these preliminaries in mind, consider first the spectra of Ag/Kr and Mn/Kr $\simeq 1/10^4$ mixtures deposited at 10–12 K, displayed in Figure 5. While the respective atomic absorptions are well separated, both the visible and UV bands of Ag_2 are coincident with Mn atomic resonance lines. Fortunately, the manganese cluster species designated Mn_x, which has been associated with a binuclear molecule, is clearly visible at 254, 317, and 410 nm, while under the high-dilution conditions employed the higher cluster species Mn_y (330–349 nm) is absent. Included in Figure 5 for the purpose of comparison is the outcome of Ag atom photoaggregation, which exhibits most of the absorptions ascribed to Ag, Ag_2, Ag_3, and some higher silver clusters.[7]

On examining the optical spectra which result from the simultaneous codeposition of Ag/Mn/Kr $\simeq 1/1/10^4$ mixtures at 10–12 K (Figure 5D), one can identify two new absorptions at 263–266 and 362 nm which cannot be associated with any of the known silver or manganese species. These two new lines have counterparts in Ag/Mn/Ar $\simeq 1/1/10^4$ experiments, absorbing at 259 and 353 nm, and would appear to be characteristic of a Ag_nMn_m bimetallic cluster. Under the high-dilution conditions employed, a weak triplet at 236/240/244 nm also appears to be associated with the Ag_nMn_m species, although the region at energies lower than 450 nm is clear after deposition. The presence of the metastable Mn′ site (290/444 nm, described earlier) under these conditions (Figure 5D) probably arises from the slightly increased thermal load in the mixed-metal experiment arising from the combined radiation of two glowing Knudsen cells.

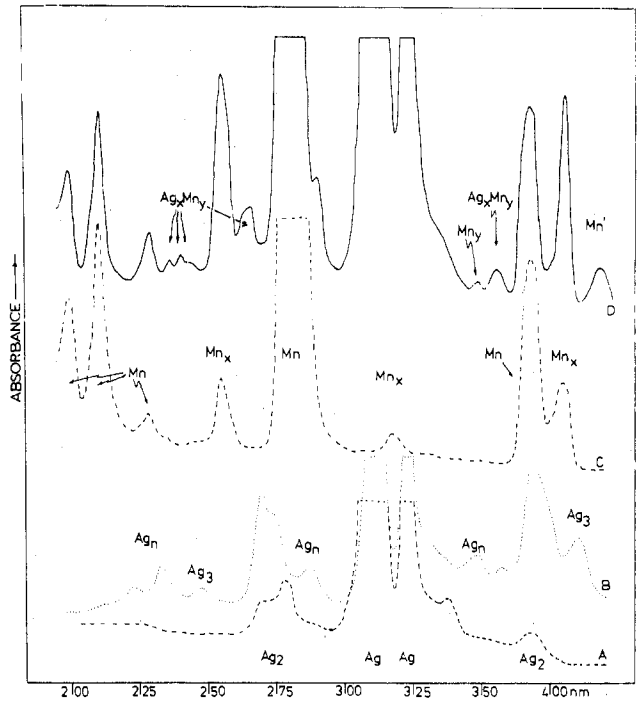

Figure 5. UV–visible spectrum of a Ag/Kr $\simeq 1/10^4$ mixture (A) at 10–12 K and (B) following silver atom photoexcitation; (C) Mn/Kr $\simeq 1/10^4$; (D) Ag/Mn/Kr $\simeq 1/1/10^4$ (see text for details).

On thermally annealing the sample shown in Figure 5D at 20 K, rapid loss of both Ag and Mn atoms with concurrent growth of the aforementioned new cluster absorptions is observed. Considering that only binuclear species should be favored under the high dispersion employed, one can tentatively associate the 263/266 and 362 nm absorptions with AgMn. It is noteworthy that the 20 K thermal annealing also causes the growth of a number of low-energy absorptions at 492, 502, 550, 592, and 604 nm which do not appear to belong to higher clusters of silver and manganese and are probably best connected to bimetallic clusters with nuclearities greater than 2. Little more can be said about these higher cluster species at this stage of the research.

Silver–Molybdenum Bimetal Vapor Studies. With use of methods similar to those described for the silver–manganese system, the optical spectra of Ag/Ar $\simeq 1/10^4$, Mo/Ar $\simeq 1/10^4$ and Ag/Mo/Ar $\simeq 1/1/10^4$ mixtures were examined for evidence of bimetallic cluster formation (Figure 6A–C, respectively). Aside from the characteristic absorptions of Ag_2 and Mo_2, the most striking observation is the appearance of a new spectral feature at 432/440 nm with a weak shoulder at 445 nm. Under the high-dispersion conditions chosen, binuclear clusters dominate as witnessed by the absence of the 245-nm absorption of Ag_3[7] and low intensity of the characteristic Mo_3 band as a shoulder on the 518-nm band of Mo_2.[1,8]

The association of the 432/440-nm band with a Ag_nMo_m species is supported by selective photoaggregation experiments. For example, irradiation of the atomic silver lines in Ag/Ar $\simeq 1/10^{3-4}$ mixtures at 10–12 K leads to the very rapid formation of sizeable amounts of Ag_2 and Ag_3.[7] However, under

(22) R. K. Nesbet, *Phys. Rev.*, **135**, A460 (1964).

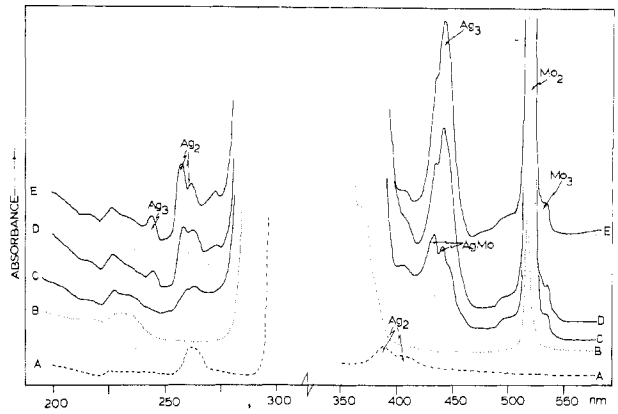

Figure 6. UV–visible spectra of (A) Ag/Ar ≃ 1/10⁴, (B) Mo/Ar ≃ 1/10⁴, and (C) Ag/Mo/Ar ≃ 1/1/10⁴ mixtures deposited at 10–12 K, showing the formation of Ag_2, Mo_2, and AgMo and (D) the result of 22-min, 318-nm Ag atom photoexcitation followed by (E) nonselective photoexcitation using broad-band irradiation.

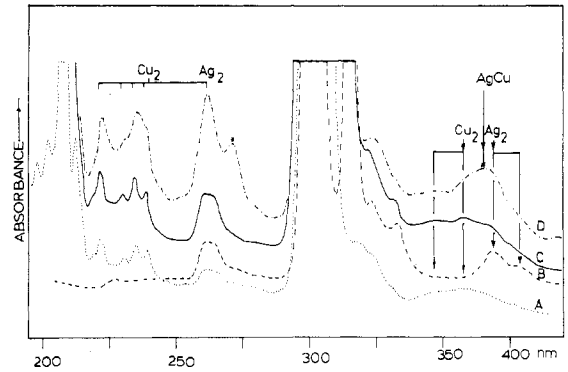

Figure 7. UV–visible spectra of (A) Cu/Ar ≃ 1/10⁴, (B) Ag/Ar ≃ 1/10⁴, and (C) Cu/Ag/Ar ≃ 1/1/10⁴ mixtures deposited at 10–12 K, indicating the spectral overlap of Ag/Cu and Ag_2/Cu_2 absorptions and (D) the result of 30-min, nonselective, 305-nm Ag/Cu atomic photoexcitation.

similar conditions in the Ag/Mo/Ar system, the presence of Mo atoms, by a mechanism that has yet to be established, impedes the silver atom photoaggregation process by at least 1 order of magnitude. Thus over a longer Ag atom irradiation period the known absorptions of Ag_2 and Ag_3, together with the new spectral feature at 432/440 nm, are observed to grow in, the latter forming a shoulder on the visible Ag_3 band (Figure 6D). Incidentally, broad-band irradiation of the Ag/Mo atomic resonances similarly exhibited slow photoaggregation behavior (Figure 6E). Although the evidence is not unequivocal, it seems reasonable under the high-dispersion conditions selected for the above experiments to associate the 432/440-nm spectral feature (intermediate in energy between those of the visible Ag_2 and Mo_2 absorptions) with the first stage of bimetallic cluster growth, namely with the species AgMo.

Silver–Copper Bimetal Vapor Studies. The clustering of silver and copper atoms in rare gas matrices by metal concentration, bulk annealing, and photoaggregation procedures has been extensively investigated by Ozin and co-workers and others.[1,6,7] From the optical spectra of Cu/Ar ≃ 1/10⁴ and Ag/Ar ≃ 1/10⁴ mixtures shown in Figure 7A,B, respectively, one can anticipate rather serious overlap problems in the corresponding Cu/Ag/Ar ≃ 1/1/10⁴ system (Figure 7C). Taking into account that the high-dispersion conditions selected for this study favor mainly atomic species and binuclear clusters on deposition, that the $^2S_{1/2} \rightarrow {}^2P_{1/2,3/2}$ resonance absorptions of Cu and Ag atoms (both sites) are essentially coincident (290–330 nm), that the valence orbital ionization potentials for Cu and Ag atoms are quite similar, and that an averaging effect[1] of Cu_2 and Ag_2 absorptions (of a similar type) might be anticipated in a AgCu bimetallic molecule, one can examine the spectra (Figure 7D) that result from Cu/Ag atom simultaneous photoexcitation (305 nm) for evidence of bimetallic clusters. The outcome of such a series of experiments points to the growth of two bands around 271 and 382 nm (marked with an asterisk in Figure 7D) which might be associated with the anticipated mixed copper–silver cluster species. As the growth of Ag_3 under these conditions is negligible and because the 382-nm absorption is essentially midway between the main visible bands of the parent diatomics Ag_2 (385/406 nm) and Cu_2 (360–370 nm), one is tempted to associate the 382-nm band with the bimetallic species AgCu. However, in view of the possibility that photoredistribution of atomic and diatomic trapping sites could confuse the issue (for example, the 272-nm band could be a secondary matrix trapping site of Cu_2[6]) the proposed assignment of AgCu absorptions must be treated with caution. Clearly, all of the bimetallic systems of the present study require further examination, by optical emission as well as other more discerning spectroscopic probes, to better define the identity of the various trapped species. However, assuming that our absorption assignments of Mn_2, AgMn, AgMo, and AgCu are reasonable, then one can begin to unravel their electronic and bonding properties by EHMO computational techniques as described in the following sections.

Extended Hückel Molecular Orbital Calculations for Mn_2, AgMn, AgMo, and AgCu. A relatively useful gateway into the electronic and bonding properties of small metal clusters involves spectroscopically parameterized EHMO computational techniques.[23,24] By making a judicious choice of parameters for molecules such as Cr_2, Mo_2, and Ag_2 so as to fit the respective electronic transitions, it is possible to arrive at reasonable bond lengths, dissociation energies, and optical transitions not only for the homonuclear molecules but also for the heteronuclear combinations CrMo and AgCr.[1,2] The method is extended to the AgMn, AgMo, and AgCu bimetallics of the present study, beginning with an examination of Mn_2, in order to further test the extent of application and usefulness of the transference of optimized EHMO parameters between related metal cluster systems.

Dimanganese. Mass spectroscopic investigations of the species present in manganese vapor indicate that Mn_2 is present in low concentrations, with a bond length (r_e = 3.8 Å), vibrational frequency (ω_e = 89 cm⁻¹), and bond dissociation energy (D_e = 7.5 ± 6 kcal mol⁻¹) consistent with a van der Waals description of the molecule.[12] Cooper et al.,[25] using EHMO methods, calculated, at r_e = 1.90 Å, D_e = 28 kcal mol⁻¹ and ω_e = 325 cm⁻¹, that is, bond properties at variance with the experimental picture of Mn_2. Nesbet's[22] ab initio HF calculations for Mn_2 represented one of the earliest, first-principles calculations of a transition-metal dimer molecule. The lowest lying electronic configuration was found to be $1\sigma_g^2 2\sigma_g^2 \pi_u^2 \pi_g^2 \delta_g^2 \delta_u^2 1\sigma_u^2$ with a bond energy of 18 kcal mol⁻¹ at 2.88 Å. Recent density functional calculations for Mn_2 by Jones and Harris[26] found the aforementioned configuration to be unbound and proposed instead $1\sigma_g^2 2\sigma_g^1 \pi_u^3 \delta_g^2 \delta_u^2 \pi_g^2 1\sigma_u^1 2\sigma_u^1$ (D_e = 28 kcal mol⁻¹, r_e = 2.66 Å) or $1\sigma_g^2 2\sigma_g^2 \pi_u^2 \delta_g^2 \delta_u^2 \pi_g^2 1\sigma_u^1 2\sigma_u^1$ (D_e = 28 kcal mol⁻¹, r_e = 2.70 Å) as ground-state configurations.

(23) (a) R. C. Baetzold, *J. Chem. Phys.*, **55**, 4355, 4363 (1971); *Adv. Catal.*, **25**, 1 (1971); (b) R. C. Baetzold and R. E. Mack, *J. Chem. Phys.*, **62**, 1513 (1975).
(24) A. B. Anderson, *J. Chem. Phys.*, **68**, 1744 (1978), and references therein.
(25) W. F. Cooper, G. A. Clarke, and C. R. Hare, *J. Phys. Chem.*, **76**, 2268 (1972).
(26) J. Harris and R. O. Jones, *J. Chem. Phys.*, **70**, 830 (1978).

Table IV. Optimized Parameters Used in Extended Hückel Calculations[a]

metal	orbital	orbital exponents	H_{ii}, eV
Mn	3p	4.036	−61.20
	3d	3.509	−7.60
	4s	1.321	−5.88
	4p	1.200	−3.00
Cu	3p	4.876	−72.70
	3d	4.201	−11.75
	4s	1.208	−7.60
	4p	1.450	−3.25
Mo	4p	3.761	−44.39
	4d	3.105	−7.00
	5s	1.409	−7.00
	5p	0.994	−4.25
Ag	4p	4.678	−69.03
	4d	3.805	−9.82
	5s	1.606	−6.52
	5p	1.354	−2.20

[a] Initial parameters taken from ref 23 and 24 and optimized by methods similar to those described in ref 1 and 2.

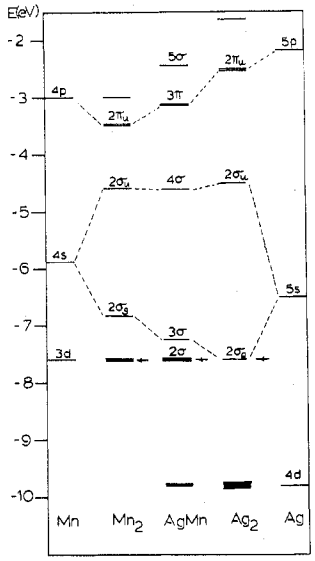

Figure 8. EHMO energy level schemes calculated for Ag_2, AgMn, and Mn_2 at their minimum energy geometries. The HOMO level is indicated by an arrow; broken lines connect related levels.

Initial EHMO calculations in the present study employing literature VOIP's and orbital exponents (Table IV) indicated a number of spin- and dipole-allowed electronic transitions at low energies originating in a closely spaced d-orbital manifold (Figure 8). With these unadjusted Mn parameters, a minimum in the ground-state Mn_2 potential curve was not found, which is not unexpected for a weakly bonded dimer. At 2.9 Å, the molecular orbital scheme of Figure 8 yields a reasonable fit with the observed optical transitions of Mn_x (Table V).

Silver–Manganese. The AgMn molecule has been observed mass spectrometrically, from which $D_e = 27 \pm 15$ kcal mol^{-1} at $r_e = 3.3$ Å has been extracted.[27] Direct transference of Mn_2 and Ag_2 EHMO parameters to AgMn resulted in the molecular orbital scheme shown in Figure 8 at the minimum-energy geometry of $r_e = 2.8$ Å. However, only a shallow potential well was observed, yielding $D_e \simeq 1$ kcal mol^{-1}, which is probably too low a value because of the underestimation of the d-orbital involvement in the bonding description of the AgMn molecule. The scheme in Figure 8 yields the correlation of calculated and observed transitions shown in Table V for the three band systems tentatively ascribed to AgMn.

(27) A. Kant, *J. Chem. Phys.*, **48**, 523 (1978).

Table V. Correlation between Calculated and Observed Electronic Transitions for Mn_2, Cu_2, Mo_2, Ag_2, AgMn, AgMo, and AgCu in Argon Matrices

molecule	r_e, Å	assignt	ν, cm^{-1} calcd (EHMO)	ν, cm^{-1} obsd[b] (argon)
Mn_2[a]	2.90	$1\sigma_g \rightarrow 2\sigma_u$	24 300	24 300
		$1\sigma_g \rightarrow 2\pi_u$	33 400	31 600
		$1\pi_u \rightarrow 3\sigma_g$	37 100	39 400
AgMn	2.80	$2\sigma \rightarrow 4\sigma$	24 000	27 600
		$2\sigma \rightarrow 3\pi$	36 100	38 000/37 600
		$2\pi \rightarrow 5\sigma$	41 500	41 700/41 000/40 300
AgMo	3.00	$2\sigma \rightarrow 4\sigma$	20 400	22 700/23 200
		$2\sigma \rightarrow 3\pi$	29 300	overlap
		$2\sigma \rightarrow 5\sigma$	42 000	overlap
Mo_2	2.20	$1\sigma_g \rightarrow 2\sigma_u$	19 400	19 300
Ag_2	2.70	$2\sigma_g \rightarrow 2\sigma_u$	24 600	24 600
		$2\sigma_g \rightarrow 2\pi_u$	40 800	38 800
AgCu	2.90	$3\sigma \rightarrow 4\sigma$	25 900	26 200
		$3\sigma \rightarrow 3\pi$	40 000	36 900
Cu_2	2.20	$2\sigma_g \rightarrow 2\sigma_u$	27 300	27 800
		$2\sigma_g \rightarrow 2\pi_u$	39 400	38 200

[a] Refers to Mn_x species (see text). [b] Accuracy of the matrix wavenumber positions estimated to be ±100 cm^{-1}.

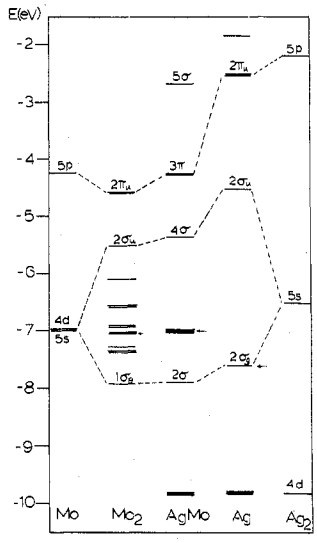

Figure 9. EHMO energy level schemes for Ag_2, AgMo, and Mo_2.

Silver–Molybdenum. With use of a similar approach to that described for AgMn, EHMO calculations were performed on AgMo by using the parameters listed in Table IV. The main contributors to the AgMo bonding arise from overlap of the Ag and Mo 5s orbitals with essentially no involvement of the respective 4d orbitals (similar to the situation found in AgCr[2]).

The minimum-energy geometry for AgMo was computed at 3.0 Å, elongated with respect to both the multiply bonded Mo_2 and singly bonded Ag_2 molecules.[1,2] Not surprisingly, the bond dissociation energy of AgMo computed at 41.8 kcal mol^{-1} was slightly less than the value obtained for Ag_2[2] (46 kcal mol^{-1}) and considerably below the Mo_2[1] (78 kcal mol^{-1}) value. From the EHMO scheme of AgMo displayed in Figure 9 one can expect three absorptions in the accessible UV–visible spectral range: $2\sigma \rightarrow 4\sigma$, 3π, 5σ (Table V). The lowest energy transition is calculated around 20 500 cm^{-1} and might be correlated with the 23200/22700-cm^{-1} doublet ascribed earlier to AgMo. Higher energy absorptions were not observed for AgMo, possibly because of overlap with atomic lines as indicated by the calculated values of the $2\sigma \rightarrow 3\pi$ and 5σ (Table V). Some credence for the AgMo assignment stems from the internal consistency of the Ag_2, AgMo, and Mo_2 observed and

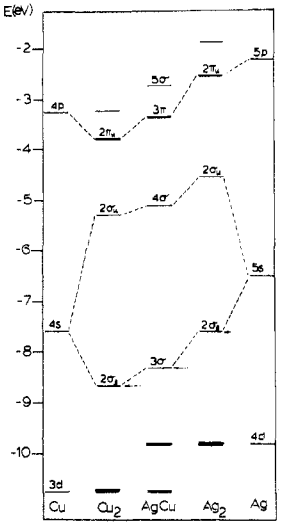

Figure 10. EHMO energy level schemes for Ag_2, AgCu, and Cu_2.

calculated optical transitions, particularly the intermediacy of the low-energy AgMo absorption between the respective absorptions of Ag_2 and Mo_2 (Figures 6 and 9, Table V).

Silver–Copper. As described earlier, the optical spectral coincidences between Ag/Cu and Ag_2/Cu_2 caused problems in the determination of the AgCu assignments. Absorptions at 382 and 271 nm are tentatively associated with the AgCu molecule. Further clarification of the system could stem from bimetallic fluorescence experiments.

Direct transfer of optimized EHMO parameters for Ag_2 and Cu_2 (Table IV) to AgCu yields the molecular orbital scheme of Figure 10 at the minimum energy distance of 2.9 Å. Three transitions can be expected within the range of our instrument, $3\sigma \rightarrow 4\sigma$, 3π, and 5σ, at energies intermediate between those of Ag_2 and Cu_2 (Table V). This averaging effect of the transition energies for AgCu relative to Ag_2 and Cu_2 is intuitively reasonable for atomic and diatomic species having $^2S_{1/2}$ and $^1\Sigma_g^+$ electronic ground states, respectively. Furthermore, the Cu (4s) and Ag (5s) orbitals have similar energies and make up the metal–metal bonds with little contribution from the 3d/4d-orbital sets, particularly in the case of silver.

On a final note, the AgCu bond dissociation energy was computed at 33 kcal mol^{-1} which is close to the 40.7 kcal mol^{-1} established mass spectrometrically[28] but slightly less than the 45 and 38 kcal mol^{-1} values determined for Cu_2 and Ag_2, respectively.

Discussion

The apparent ease with which certain atomic components participate in bimetallic cluster formation at the scale of just a few atoms, especially for combinations such as Ag/Cr, Ag/Mo, and Ag/Mn, which from their bulk-phase diagram comprise the class of immiscible alloys, brings to the forefront the question of whether any two metal atomic components can form heteronuclear cluster molecules. In a practical sense, these studies are of considerable significance in view of the work of Sinfelt[3] and others with high-dispersion, multicomponent particle catalysts (10–1000 Å), composed of totally or partially miscible metal constituents in the bulk state. Supported and unsupported catalysts of this type often display remarkably distinct chemical properties from those of the individual metals and led Sinfelt and others to view them as "bimetallic" rather than "alloy" cluster catalysts.[3] In this context, the term "bimetallic" implies an electronic interactive model, rather than one comprising a simple addition or superposition of the properties of the individual atom–cluster components.

The results of bimetallic cluster growth in a region of two or three metal atomic components, for example, CrMo, $CrMo_2$, Cr_2Mo,[1] AgCr, Ag_2Cr,[2] NbMo,[29] AgMo, and AgMn, convey the image that these metal molecules are "normal" in an electronic, optical, bonding and probably a chemical sense. The most significant aspect of these studies is probably that such bimetallic cluster molecules can actually be fabricated. Recall that the respective bulk alloy systems are of the immiscible or partially miscible class, and hence the small cluster results can be considered to lend further credence to Sinfelt's[3] proposal of a direct interaction between metallic components in the respective multicomponent, very small particle systems.

In contrast, one must be alert to the fact that straightforward mixing of metal atomic components does not necessitate bimetallic cluster growth at the few-atom level of operation, as witnessed by the optical spectra of Ag/Pd, Ag/Pt, Pd/Mo, and Ag/Ru,[4,10] which display just the additive features of the atomic and diatomic components. Clearly, a more thorough appreciation of metal atom–cluster nucleation phenomena under low-temperature conditions requires a detailed understanding of the electronic configurational alterations and kinetic barriers which make up the complex sequence of events leading up to the nucleation and growth of bimetallic molecules. Research is continuing along these lines, with use of other spectroscopic probes. Extensions to polymer-supported unimetallic, bimetallic, and trimetallic cluster compositions are already under development,[30] and the stage is now set for an excursion to the selective chemical reactions of small M_nM_m' cluster molecules with reactive ligands. The latter investigations are likely to generate valuable data on (i) preferred sites of ligand coordination, (ii) alterations in cluster and ligand properties on complexation, and (iii) relationships to and differences from the situation of the ligand chemisorbed on bulk, bimetallic particle, or alloy surfaces. Studies of this type, at the atomic scale of operation, might illuminate present concepts of "electronic and geometrical" factors in catalysis.[31]

Acknowledgment. We gratefully acknowledge the financial assistance of the National Research Council of Canada's Operating, New Ideas and Strategic Energy Programs, Imperial Oil of Canada, Erindale College, and Lash Miller Chemical Laboratories for support of this research.

Registry No. Ag_2, 12187-06-3; Ag_3, 12595-26-5; Ag_4, 64475-45-2; Ag_5, 64475-46-3; Ag_6, 64475-47-4; AgMo, 74947-91-4; Mo_2, 12596-54-2; AgCu, 12249-45-5; Cu_2, 12190-70-4; Mn_2, 12596-53-1; AgMn, 12330-15-3; Mn, 7439-96-5; Cu, 7440-50-8; Mo, 7439-98-7; Ag, 7440-22-4.

(28) M. Ackerman, F. E. Stafford, and J. Drowart, *J. Chem. Phys.*, **33**, 1784 (1960).
(29) W. E. Klotzbücher and G. A. Ozin, *Inorg. Chem.*, in press.
(30) C. G. Francis, H. Huber, and G. A. Ozin, *J. Am. Chem. Soc.*, **101**, 625 (1979); *Inorg. Chem.*, **19**, 219 (1980); Proceedings of the EUCHMOS Meeting, Frankfurt, Sept 1979, published in "Spectroscopy in Chemistry and Physics", Elsevier, New York, 1979, and *J. Mol. Struct.*, **59**, 55, 1980; *Angew. Chem., Int Ed. Engl.*, **19**, 402 (1980).
(31) NBS *Spec. Publ. (U.S.)*, **No. 475** (1977), and references cited therein.